Abdominal Radiology (2025) 50:3435–3446
https://doi.org/10.1007/s00261-025-04807-0

RESEARCH

Spectral CT radiomics features of the tumor and perigastric adipose tissue can predict lymph node metastasis in gastric cancer

Zhen Zhang[1] · Xiaoping Zhao[2] · Jingfeng Gu[3] · Xuelian Chen[1] · Hongyan Wang[1] · Simin Zuo[4] · Mengzhe Zuo[3] · Jianliang Wang[1]

Received: 13 November 2024 / Revised: 8 January 2025 / Accepted: 11 January 2025 / Published online: 25 January 2025

Abstract

Objectives To develop a nomogram based on the radiomics features of tumour and perigastric adipose tissue adjacent to the tumor in dual-layer spectral detector computed tomography (DLCT) for lymph node metastasis (LNM) prediction in gastric cancer (GC).

Methods A retrospective analysis was conducted on 175 patients with gastric adenocarcinoma. They were divided into training cohort ($n=125$) and validation cohort ($n=50$). The radiomics features from the tumour and perigastric fat based on DLCT spectral images were extracted to construct radiomics models for LNM prediction using Lasso-GLM method. Preoperative clinicopathological features, DLCT routine parameters, and the optimal radiomics models were analyzed to establish the clinical-DLCT model, clinical-DLCT-radiomics model and a nomogram. All models were internally validated using the Bootstrap method and evaluated using receiver operating characteristic (ROC) curve.

Results The area under the ROC curve (AUC) values of optimal radiomics models based on tumour (Model 1) and perigastric fat (Model 2) were 0.923 and 0.822 in training cohort, 0.821 and 0.767 in validation cohort. The clinical-DLCT model based on Nct and ECV_{ID} demonstrated an AUC value of 0.728 in training cohort and 0.657 in validation cohort. The clinical-DLCT-radiomics model and the nomogram were established by incorporating Nct, ECV_{ID} and the linear predictive values of Models 1 and 2, exhibiting superior predictive efficacy with an AUC value of 0.935 in training cohort and 0.876 invalidation cohort.

Conclusions The nomogram based on Nct, ECV_{ID}, and the radiomics features of tumour and perigastric fat in DLCT demonstrates potential for predicting LNM in GC. This approach may contribute to the development of treatment strategies and improve the clinical outcomes for GC patients.

Keywords Radiomics · Perigastric adipose tissue · Dual-layer spectral detector CT · Lymph node metastasis · Extracellular volume fraction · Gastric cancer

✉ Mengzhe Zuo
15862368856@163.com

✉ Jianliang Wang
wjlks@sina.com

Zhen Zhang
403454430@qq.com

Xiaoping Zhao
99856252@qq.com

Jingfeng Gu
gujingfeng1985@163.com

Xuelian Chen
Chenxuelian0525@outlook.com

Hongyan Wang
anne5214@163.com

Simin Zuo
279807175@qq.com

[1] Department of Radiology, Affiliated Kunshan Hospital of Jiangsu University, Kunshan, China

[2] Department of Radiology, Affiliated The Fifth People's Hospital of Kunshan, Kunshan, China

[3] Department of Radiology, Kunshan Women and Children's Healthcare Hospital, Kunshan, China

[4] Department of Data Science, University of Melbourne, Melbourne, Australia

Introduction

Gastric cancer (GC) is a highly lethal malignancy, ranking third in incidence and second in mortality in China [1]. GC patients often diagnosed at advanced stages characterised by high rates of lymph node metastasis (LNM), which serves as the primary mode of spread for this disease [2, 3]. Early gastric resection combined with lymph node dissection can significantly improve patient prognosis, while accurate preoperative evaluation of LNM plays a crucial role in identifying suitable candidates and selecting optimal treatment strategies, as well as for prognostic evaluation among GC patients [4].

Multi-detector computed tomography serves as the primary imaging modality for the preoperative assessment of GC [5]. However, this subjective imaging technique lacks sufficient accuracy in identifying LNM based solely on morphology and enhancement patterns, often making it challenging to detect small or occult lymph node micrometastases, resulting in an overall evaluation accuracy of only approximately 60% [6]. Dual-layer spectral detector computed tomography (DLCT) can not only provide clear subjective images but also relevant quantitative spectral parameters, thereby offering valuable quantitative references for disease diagnosis and treatment evaluation [7]. Several studies have substantiated the clinical significance of the quantitative parameters in the preoperative assessment of LNM in GC [7]. Furthermore, there are derived quantitative parameters based on ID image data, such as extracellular volume fraction (fECV), which also exhibit substantial diagnostic value for various malignant tumours [8, 9]. However, there are few studies on the fECV for LNM evaluation in GC.

The perigastric fat, as a part of visceral adipose tissue (VAT), can potentially facilitate tumour progression by secreting various adipokines and cytokines that impact tumour biology and contribute to cancer occurrence and development, ultimately leading to unfavourable prognosis [10]. Studies have demonstrated that fat cells can promote extensive metastasis of GC, including omental and peritoneal metastases [11]. Currently, relevant research has analyzed the quantity and composition of adipose tissues for predicting tumour aggressiveness and prognosis [12]. However, tissue biopsy are often used for lipid composition analysis, which are invasive and time-consuming procedures. Therefore, there is an urgent need for a non-invasive approach capable of characterising fat composition features to indirectly evaluate tumours.

In the era of precision medicine, radiomics transforms high-resolution images into high-dimensional and minable data with multiple channels, enabling the extraction of quantitative feature information that reflects the heterogeneity of tumour characteristics [13, 14]. While current radiomics studies primarily utilise conventional mixed-energy images from routine CT scans for feature extraction, DLCT can provide different spectral images, thereby expanding the research content of radiomics and enhancing its application value in tumour evaluation [15]. Some studies have confirmed that the radiomics features of peritumoral adipose tissue can improve the value of tumor radiomics features alone in tumor evaluation [16, 17]. To date, there has been no report exist to explore the potential of radiomics features based on tumours and perigastric fat combined with quantitative parameters of DLCT for LNM prediction in GC.

In this study, artificial intelligence analysis software will be employed to extract radiomics features of tumours and perigastric fat adjacent to the tumor in gastric adenocarcinoma from multiple parameter images in DLCT and construct radiomics models. Subsequently, a nomogram will be generated by integrating meaningful clinicopathological features, routine DLCT parameters, and radiomics models for the preoperative prediction of LNM in GC.

Materials and methods

Study population

This study was approved by the Ethics Committee, and each subject signed an "Informed Consent about Contrast-Enhanced CT." A retrospective review was conducted on a cohort of 216 patients with GC who underwent endoscopy examination and DLCT prior to radical gastrectomy between June 2021 and December 2023. The inclusion criteria and exclusion criteria were listed in Supplemental Material A. Ultimately, a total of 175 eligible patients were enrolled in the study (Fig. 1). All patients were first split into training cohort and validation cohort with a ratio of 7:3 by using the random series generated by the computer. The training cohort was utilised for both model training and internal validation.

The following variables were recorded: age, gender, serum tumour markers (CEA, CA199, and CA125), endoscopic tumour location, endoscopic differentiation grade, and endoscopic pathological type.

DLCT scanning method and parameters

The DLCT scanner (IQon Spectral CT, Philips Health Systems) was utilised to perform an unenhanced scan followed by three phases of enhanced scans. Patients were instructed to consume 800–1200 ml of warm water 20 min prior to the examination, and receive an intramuscular injection of 20 mg of 654-2 for gastrointestinal peristalsis inhibition.

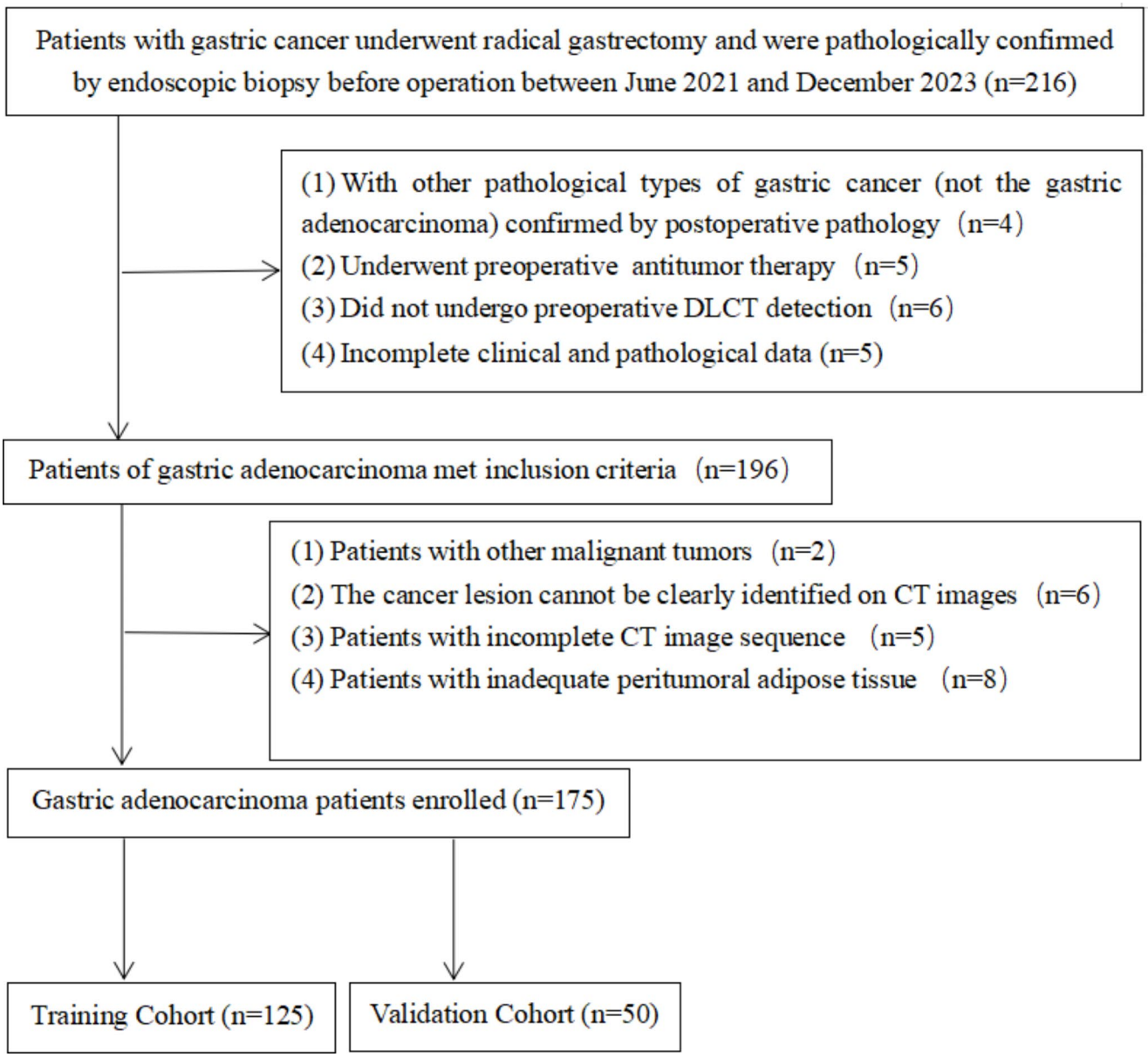

Fig. 1 Flowchart of patient enrollment

The ionic contrast medium (iohexol, Omnipaque 350) was administered intravenously at a dose of 1.5 mL/kg body weight at a rate of 3.0–3.5 mL/s, followed by 10 mL of saline at the same rate. The arterial phase, venous phase, and equilibrium phase images were acquired at 35s, 70s, and 180s post-contrast agent injection, respectively. Scanning parameters included a tube voltage of 120 kV, automatic mAs for tube current (reference value: 129mAs), pitch of 1.016, rotation time of 0.5s, scanning matrix size of 512 × 512, scanning layer thickness and spacing both set at 5 mm, and reconstruction layer thickness and spacing both set at 1 mm.

Image reconstruction and postprocessing

The arterial, venous, and equilibrium phase SBI images were imported into the Philips Image Workstation (IntelliSpace Portal version 9, Philips Healthcare) for analysis. Subsequently, 40 keV mono-energy images as well as iodine density ((ID) and effective atomic number (Zeff) images were acquired. Two radiologists with 5 and 10 years of experience independently delineated the regions of interest (ROI) on the cancer lesion in the venous phase images without access to clinical information or pathological results. The details of ROIs profiling and measurement of quantitative

parameters were listed in Supplemental Material B and shown in Figure S1A-S1D.

In addition, routine DLCT parameters including tumour thickness, T-stage assessment in CT images (T-ct), and lymph node status evaluation in CT images (Nct) were also obtained. Tumour thickness is defined as the perpendicular distance from the major axis at its largest level. T-ct was evaluated based on the TNM staging system criteria from UICC/AJCC 8th edition [18]. Nct positivity was determined by a minimum lymph node diameter was larger than 6 mm for perigastric LN and larger than 8 mm for extraperigastric LN observed on mixed-energy CT images [18]. Two abdominal imaging experts with 5 and 10 years of experience independently assessed these parameters without knowledge of pathological results. In cases where their evaluations were inconsistent, final assessments were made through joint discussion and negotiation.

Radiomics workflow

Image segmentation

The image segmentation and feature extraction process utilised mixed-energy images, 40 keV mono-energy images, and ID images from both arterial and venous phases. Two radiologists with 6 and 8 years of experience in abdominal CT diagnosis who were blinded to the clinical and histopathological data except for the general location of the tumor performed the annotation of data on the mixed-energy images using artificial intelligence-assisted diagnosis modelling software (AIMS). The details of segmentation were in Supplemental Material C. ROIs were obtained for both the tumour and perigastric fat in arterial and venous phase images, resulting in a total of 4 ROIs on each type of images and 12 ROIs in each patient for feature extraction (Figure S2).

A reliability test was performed to guarantee the reproducibility and robustness of the radiomics features (Supplemental Material D).

Feature extraction and selection

Utilising the "feature extraction" module of AIMS, the images were reconstructed using a Laplacian-Gaussian (LoG) filter with sigma values of 4 and 5 mm, respectively. Subsequently, Wavelet transform and LoG transform were applied to extract features based on the original image characteristics. The extracted features encompassed first-order statistics, shape descriptors, and texture measures, including GLCM, GLRLM, GLSZM, NGTDM, and GLDM. Following extraction, all features were standardised using z-score normalization.

Features with a correlation coefficient (ICC) greater than 0.8 in the reliability test were subsequently included in further selection processes. The "feature selection" module of AIMS was used to employ the least absolute shrinkage and selection operator (LASSO) regression analysis method, and then features from three single-parameter images in both arterial and venous phases were individually selected. Key features for predicting LNM of gastric adenocarcinoma were determined, and a 10-fold cross-validation approach was employed to select the most appropriate λ value. Finally, optimal features along with their corresponding coefficients were obtained.

Radiomics modelling

The image features of tumour and perigastric fat from single-parameter images and multi-parameter images were used to construct generalised linear models (GLM) for predicting LNM of GC using the "modelling" module of AIMS. In total, eight models (mix-tumour model, 40 keV-tumour model, ID-tumour model, combined-tumour model, mix-fat model, 40 keV-fat model, ID-fat model, and combined-fat model) were developed. The area under the operating characteristic (ROC) curve (AUC) values of the eight models were compared to select the optimal models based on tumour and perigastric fat, respectively. The optimal models were further validated using the Bootstrap method with 1000 resamples. Finally, the linear predictive values of the optimal models were obtained. The workflow of the DLCT-based radiomics analysis was illustrated in Fig. 2.

Statistical analysis

Statistical analysis was conducted using SPSS 19.0, MedCalc 15.0, and R software packages (version 4.0.5, http://www.Rproject.org). The normality of the distribution was assessed using the K-S test. Continuous variables with normal distribution were expressed as mean ± standard deviation, while those without normal distribution were expressed as median (interquartile range). Categorical variables were presented as n (%). The differences in clinicopathological and routine DLCT parameters between the LNM and non-LNM group were analyzed using the independent sample t-test or Wilcoxon test for continuous variables, and the Chi-square test or Fisher's exact test for categorical variables. Multivariate logistic regression backward stepwise analysis was employed to identify independent predictors of LNM in GC and to construct the clinical-DLCT model and the clinical-DLCT-radiomics model. Parameters with p-value < 0.05 were considered statistically significant in the multivariate analysis. The ROC curve analysis and Delong test were used to compare the predictive efficacy of each model. The

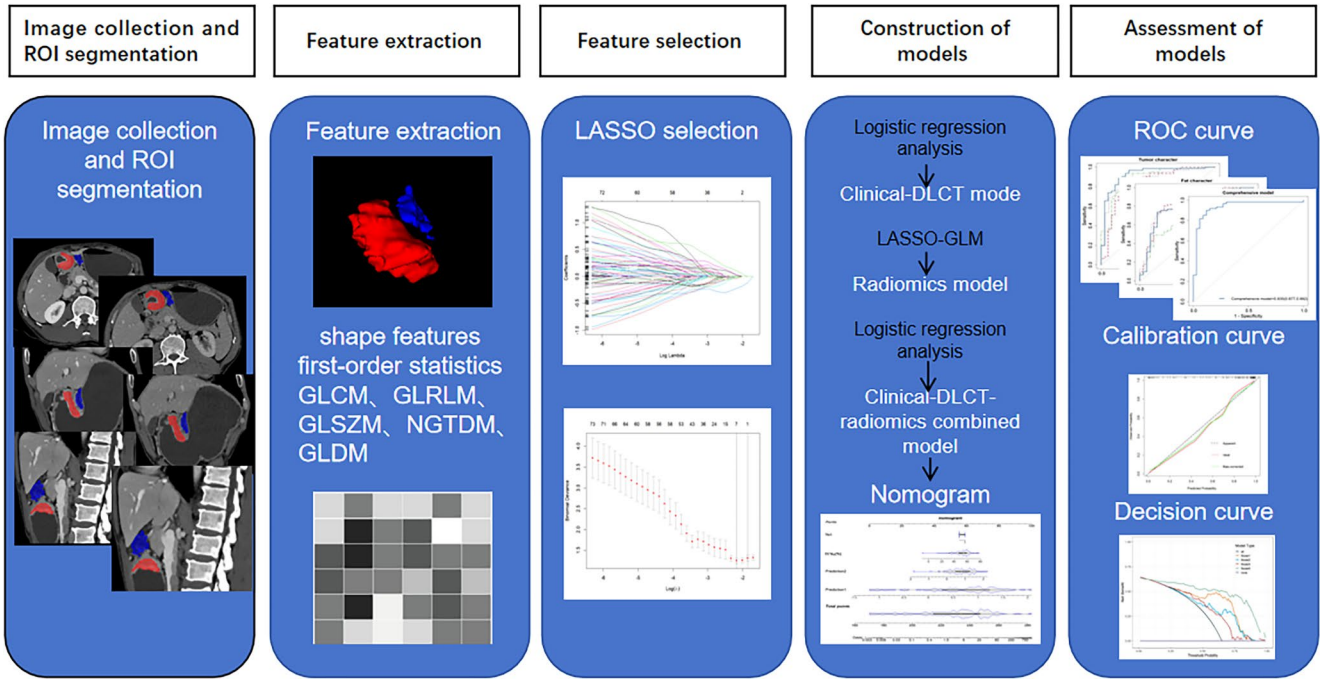

Fig. 2 Workflow of the DLCT-based radiomics analysis. Following segmentation of tumor and perigastric areas in the acquired images, radiomics features were extracted for each patient. The LASSO algorithm was used to select pertinent radiomics features, which were subsequently subjected to linear fitting to construct radiomics models. Logistic regression analysis was employed to develop both clinical-DLCT and clinical-DLCT-radiomics combined models. Model performance was evaluated using ROC curves, calibration curves, and decision curve analysis (DCA)

R software was used to generate a nomogram. The calibration of the nomogram was evaluated by calibration curves using the Hosmer-Lemeshow test. The clinical applicability of each model was assessed using decision curve analysis (DCA). A p-value < 0.05 indicated statistically significance.

Results

Patient characteristics

A total of 175 patients with gastric adenocarcinoma were included in this study and divided into training cohort 125 cases and validation cohort 50 cases, comprising 113 patients with LNM and 62 patients without LNM. Among the participants, there were 126 males and 49 females, with ages ranging from 34 to 88 years (mean age: 68.51 ± 9.97 years). The clinicopathological characteristics of the enrolled patients are presented in Table 1.

Radiomics model

Radiomics models based on tumor

A total of 2,292 features from the images of tumour with an inter-observer ICC value > 0.8 were included in the analysis. Lasso regression analysis was employed for feature selection, as illustrated in Figure S3. The selected features were included to construct four radiomics models based on the three single-parameter images and multi-parameter images, respectively (Figure S4). Among the four models, the model incorporating multi-parameter image features (Model 1) demonstrated superior diagnostic efficiency in the training cohort (Fig. 3A). The internal and independent validation ROC curves were shown in Fig. 3B and C.

Radiomics models based on perigastric fat

A total of 1,850 features from the images of perigastric fat with an inter-observer ICC value > 0.8 were included in the analysis. Lasso regression analysis was employed for feature selection, as illustrated in Figure S5. The selected features were included to construct four radiomics models based on the three single-parameter images and multi-parameter images, respectively (Figure S6). Among the four models, the ID images feature model (Model 2) demonstrated superior diagnostic efficiency in the training cohort (Fig. 3D). The internal and independent validation ROC curves were shown in Fig. 3E and F.

Table 1 Comparison of preoperative clinicopathological features and routine DLCT parameters between LNM and non-LNM groups

	Training Cohort				Validation Cohort			
Feature	LNM(-) (n=45)	LNM(+) (n=80)	t/Z/χ^2	p	LNM(-) (n=17)	LNM(+) (n=33)	t/Z/χ^2	p
Age(year)	68.18±8.71	68.69±11.35	0.223[a]	0.824	71.24±9.22	66.85±13.30	1.215[a]	0.230
Gender			0.012[c]	0.913			1.532[c]	0.216
Male	32 (71.1%).	59 (73.8%).			10(58.82%)	25(75.76%)		
female	13 (28.9%).	21 (26.3%).			7(41.18%)	8(24.24%)		
Endoscopic pathological type			4.768[c]	0.18			0.003[c]	0.622
Tubular adenocarcinoma	32 (71.1%).	57 (71.3%).			12(70.59%)	22(66.67%)		
Non-tubular adenocarcinoma	13 (28.9%).	23 (28.8%).			5(29.41%)	11(33.33%)		
Endoscopic differentiated degree			4.414[c]	0.036*			1.156[c]	0.282
Low differentiation	8 (17.8%)	31 (38.8%).			11(64.71%)	26(78.79%)		
Moderate-high differentiation	37 (82.2%)	49 (61.3%).			6(35.29%)	7(21.21%)		
Endoscopic tumor location			3.280[c]	0.353			5.558[c]	0.137
Cardia or fundus	10 (22.2%)	28 (35.0%).			3(17.65%)	15(45.45%)		
Body of stomach	7 (15.6%)	17 (21.3%).			5(29.41%)	4(12.12%)		
Antrum or pylorus	23 (51.1%).	24 (30.0%).			7(41.18%)	8(24.24%)		
Overlapping sites	5 (11.1%)	11 (13.8%).			2(11.76%)	6(18.18%)		
Serum tumor marker								
CEA(ng/ml)			2.026[c]	0.155			1.418[c]	0.328
≤5	37(82.2%)	58(72.5%)			12(70.6%)	22(66.7%)		
>5	8(17.8%)	22(27.5%)			5(29.4%)	11(33.3%)		
CA199(U/ml)			3.670[c]	0.055			0.595[c]	0.702
≤30	39(86.7%)	59(73.8%)			13(76.5%)	25(75.8%)		
>30	6(13.3%)	21(26.3%)			4(23.5%)	8(24.2%)		
CA125(U/ml)			0.002[c]	0.963			1.495[c]	0.234
≤25	36(80%)	65(81.3%)			12(70.6%)	26(78.8%)		
>25	9(20%)	15(18.8%)			5(29.4%)	7(21.2%)		
Nct			10.986[c]	0.001*			8.642[c]	0.003*
negative	30 (66.7%)	23 (28.8%).			12(70.59%)	9(27.27%)		
positive	15 (33.3%).	57 (71.3%).			5(29.41%)	4(72.72%)		
Tumor Thickness(mm)	16.60 (13.65, 19.60)	19.10 (15.75, 23.35)	2.602[b]	0.005*	19.27±12.11	19.39±13.30	-0.044[a]	0.965
APCT40kev(Hu)	163.6 (117.55, 213.55)	157.2 (118.40, 201.35)	0.368[b]	0.713	168.10 (147.40, 214.80)	159.20 (116.65, 223.28)	-1.137[b]	0.256
VPCT40kev(Hu)	200.90±54.03	201.69±53.59	0.068[a]	0.946	198.40 (157.80, 232.80)	186.90 (165.58, 237.78)	-0.020[b]	0.984
DPCT40kev(Hu)	177.32±47.24	187.57±40.57	1.102[a]	0.273	171.32±43.81	182.94±40.82	-0.930[a]	0.357
APZeff	8.11 (7.86, 8.35)	8.11 (7.86, 8.33)	0.313[b]	0.754	8.17 (8.04, 8.26)	8.08 (7.87, 8.44)	-1.168[b]	0.243
VPZeff	8.31 (8.10, 8.49)	8.34 (8.11, 8.54)	0.309[b]	0.757	8.24 (8.14, 8.47)	8.27 (8.14, 8.48)	-0.164[b]	0.870
DPZeff	8.16 (8.02, 8.33)	8.22 (8.16, 8.46)	1.510[b]	0.131	8.17±0.25	8.23±0.22	-0.972[a]	0.336
APNID	0.13 (0.10, 0.21)	0.12 (0.08, 0.17)	1.397[b]	0.163	0.15 (0.11, 0.16)	0.12 (0.10, 0.21)	-0.563[b]	0.573
VPNID	0.43 (0.35, 0.54)	0.43 (0.33, 0.55)	0.408[b]	0.683	0.42 (0.39, 0.50)	0.43 (0.37, 0.61)	-0.420[b]	0.675
DPNID	0.52 (0.48, 0.67)	0.60 (0.50, 0.71)	1.260[b]	0.208	0.50 (0.42, 0.65)	0.65 (0.51, 0.80)	-2.161[b]	0.031*
ECV_{ID}(%)	34.88 (32.04, 39.08)	40.36 (36.27, 46.57)	2.808[b]	0.002*	34.85±8.95	43.27±9.11	-3.113[a]	0.003*
T-ct			9.482[c]	0.009*			7.134[c]	0.013*
T1/T2	20 (44.4%).	7 (8.8%)			6(35.29%)	2(6.06%)		
T3/T4	25 (55.6%).	73(91.3%).			11(64.71%)	31(93.94%)		

Note: a stands for t value, b for Z value, and c for χ^2 value

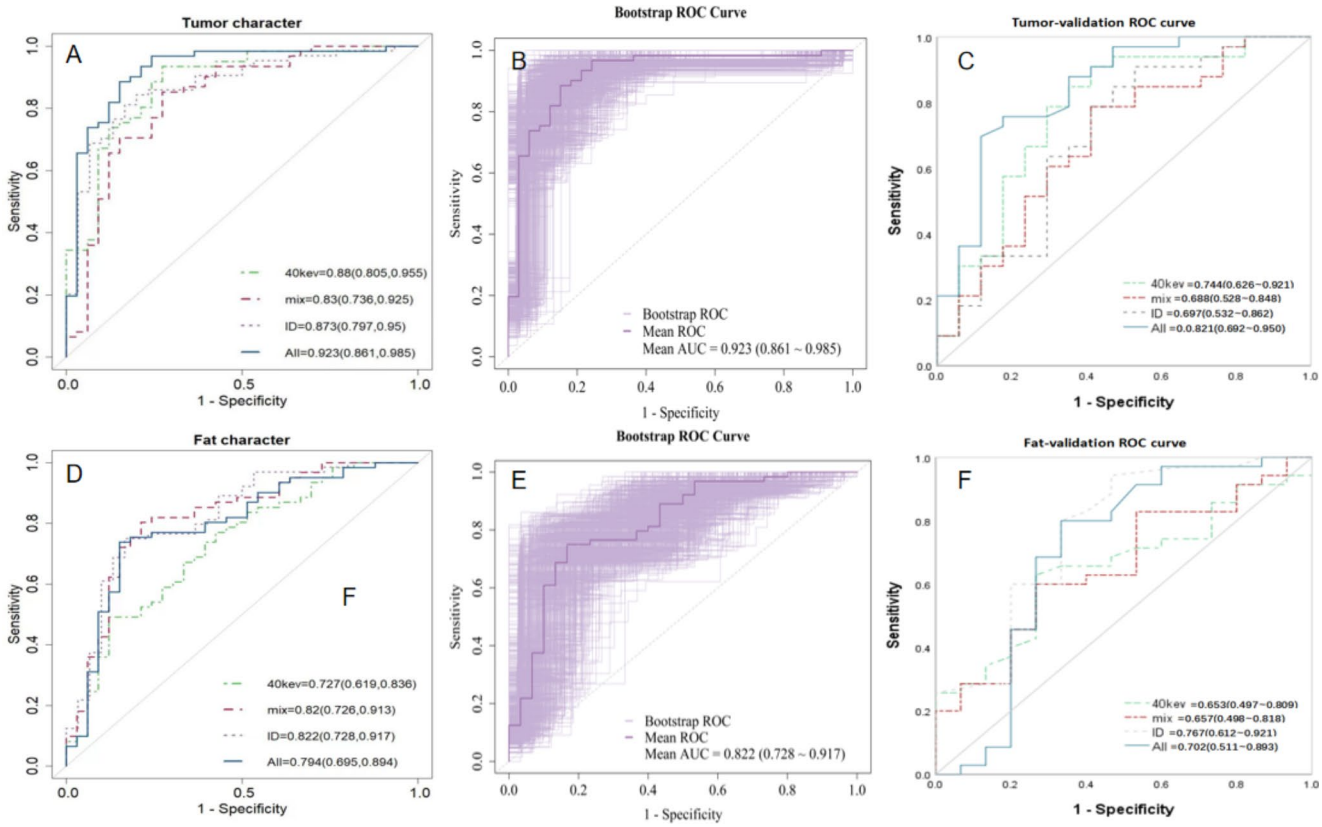

Fig. 3 ROC curves of radiomics models in the training and validation cohort. (**A, D**) ROC curves of radiomics models based on the mixed-energy images, 40 keV mono-energy images, ID images, and all image features of tumour and perigastric fat in the training cohort. Among them, the multi-parameters images models based on tumour (Model 1) and ID images models based on perigastric fat (Model 2) demonstrated superior diagnostic performance for LNM prediction. (**B, E**) Bootstrap internal validation ROC curves of Model 1 and Model 2 in the training cohort. (**C, F**) ROC curves of radiomics models based on the mixed-energy images, 40 keV mono-energy images, ID images, and all image features of tumour and perigastric fat in the validation cohort. Among them, the multi-parameters images models based on tumour (Model 1) and ID images models based on perigastric fat (Model 2) demonstrated superior diagnostic performance for LNM prediction

Clinical-DLCT model

In the preoperative clinicopathological features and routine DLCT parameters, the endoscopic differentiation degree, Nct, tumour thickness, T-ct, and ECV_{ID} exhibited statistically differences between the LNM and non-LNM group in the training cohort (all $P<0.05$) (Table 1). Multivariate logistic regression analysis revealed that Nct and ECV_{ID} were independent predictors of LNM in GC with the OR values of 3.634 (95%CI: 1.428–9.251) and 1.102 (95%CI: 1.005–1.208), respectively ($p<0.05$). A clinical-DLCT model (Model 3) was established incorporating Nct and ECV_{ID}, with the ROC curves of training and validation cohort shown in Fig. 4A and C.

Clinical-DLCT-radiomics model and nomogram

The linear predictive values of the two optimal radiomics models for tumour and perigastric fat (Model 1 and Model 2), along with the independent predictors (Nct and ECV_{ID}), were combined to construct the clinical-DLCT-radiomics model (Model 4). The ROC curves of training and validation cohort were shown in Fig. 4D and F. Subsequently, a nomogram was concurrently generated (Fig. 5A).

Assessment of model performance

As Table 2 shows, in the training cohort, the AUC of Model 4 was higher than that of other models, and the differences between Model 4 and Model 2, 3 were statistically significant (Z=-0.113 and −0.207, $p<0.05$), but no significant difference was observed between Model 4 and Model 1 (Z=-0.012, $p=0.783$). In the validation cohort, the AUC of the Model 4 was also higher than that of other models, and the differences between Model 4 and Model 3 was statistically significant (Z=2.345, $p<0.05$), but no significant difference was observed between Model 1 and other models (Z=0.929 and 1.338, $p=0.353$ and 0.181). The ROC curve analysis showed that when the threshold of model 4 was 0.664, the Youden index of the model was the largest, and

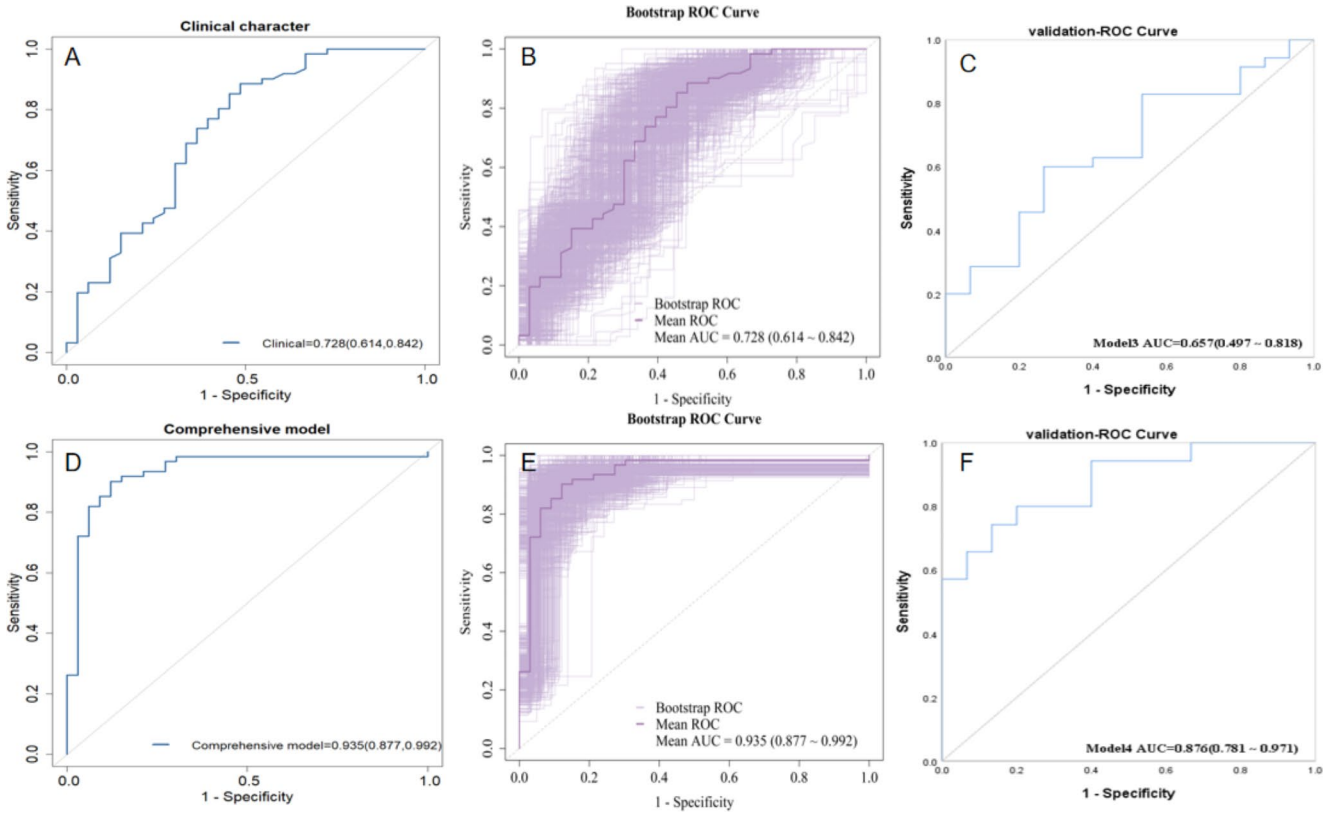

Fig. 4 ROC curves of clinical-DLCT model and clinical-DLCT-radiomics model in the training and validation cohort. (**A, D**) ROC curves of clinical-DLCT model (Model 3) and clinical-DLCT-radiomics model (Model 4) in the training cohort. (**B, E**) Bootstrap internal validation ROC curves of Model 3 and Model 4 in the training cohort. (**C, F**) ROC curves of Model 3 and Model 4 in the validation cohort

the sensitivity and specificity of the model reached the best balance. Notably, Model 4 displayed higher sensitivity, specificity, and accuracy in predicting LNM in GC with an cut-off value of 0.664 than the other three models both in the training and validation cohort.

The nomogram calibration curves demonstrated good agreement between observed and predicted outcomes in the two cohorts (Hosmer-Lemeshow test, $p = 0.426$ and 0.513) (Fig. 5B). DCA revealed that Model 4 exhibited superior net clinical benefit in predicting LNM in GC compared to the other three models in the training cohort (Fig. 5C). A typical case in which this nomogram was applied is shown in Figure S7.

A stratification analysis on the subgroups of tumor location and pathological T stage (pT-stage) was performed to explore the robustness of the nomogram. Detailed description on stratified analysis is provided in Supplemental Material E. The results showed that the diagnostic efficiency of nomogram was not affected by the tumor location and pT-stage (DeLong test, all $p > 0.05$) (Figure S8), suggesting its robustness on different subgroups of GC.

Discussion

In this study, the radiomics models based on multi-parameter images of tumours and ID images of perigastric fat were constructed and demonstrated superior diagnostic performance for LNM in GC. Then, a clinical-DLCT model was established using Nct and ECV_{ID} as independent predictors of LNM in GC. Finally, a clinical-DLCT-radiomics model and the corresponding nomogram were generated by integrating the two best radiomics models, Nct, and ECV_{ID}. The predictive performance and clinical application value of the nomogram for LNM in GC surpassed that of other models.

Currently, numerous studies have utilised CT images of GC lesions to establish radiomics models for predicting LNM [19]. However, these studies rely solely on mixed-energy images, limiting the image sources used for feature extraction and resulting in a lack of richness in obtained radiomics features. In this study, DLCT provided not only conventional mixed-energy images but also spectral images. Li et al. [20] extracted features from mono-energy images of dual-energy CT to establish a deep learning model that exhibits greater predictive value for LNM in GC compared to single-parameter image models. However, the mix-energy

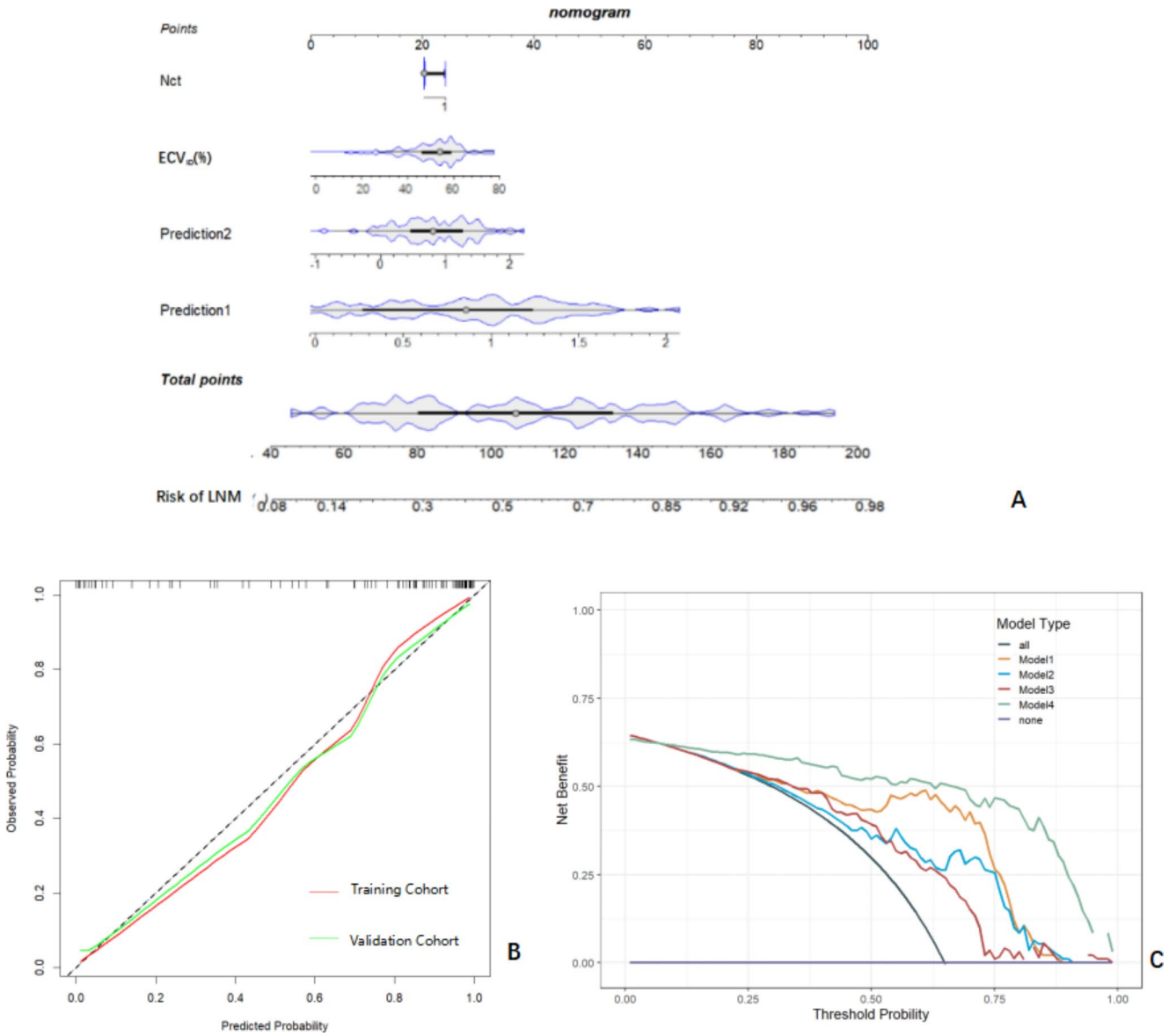

Fig. 5 (**A**) Nomogram constructed from Nct, ECV_{ID} and the linear predictive values of Model 1 and Model 2. (**B**) The calibration curve of the nomogram in the training and validation cohort. (**C**) The DCA of the four models in the training cohort: the threshold probability is shown on the X-axis, and the net benefit is shown on the Y-axis

images and ID image features were not included in this study. Thus, our research constructed a multi-parameter radiomics model from combined features of mixed-energy images, 40 keV mono-energy images, and ID images of GC lesions. The model outperformed the single-parameter models by better capturing the heterogeneity and aggressiveness of GC lesions and offered a more optimised approach than traditional enhanced CT.

Cancer-associated adipose tissue can promote tumor cell growth, proliferation, invasion, and metastasis by altering lipid metabolism within cancer cells, releasing pro-inflammatory cytokines and tumor adipokines, facilitating extracellular matrix remodelling, and providing various metabolic substrates [21–23]. The changes in the molecular profile of adipose tissue surrounding the tumor can influence the radiomics features of corresponding images, which may not be apparent through visual assessment alone [17]. Jayaprakasam et al. [17] analysed radiomics features of mesorectal fat in MRI images of rectal cancer, finding these features predictive of pathological complete response, local and distant recurrence, as well as T and N stages after treatment, underscoring the importance of cancer-associated adipose tissue characteristics in assessing tumor heterogeneity and aggressiveness. In recent years, several studies have highlighted a strong correlation between visceral fat and LNM in GC [24]. Currently, there was few fat-based

Table 2 Comparison of AUC, sensitivity, specificity and accuracy among the four models in the training and validation cohort

	Model	AUC (95%CI)	Sensitivity (95%CI)	Specificity (95%CI)	Accuracy	Cut-off value
Training Cohort	Model1	0.923 (0.861 ~ 0.985)	0.885 (0.821 ~ 0.949)	0.848 (0.775 ~ 0.921)	0.872	0.635
	Model2	0.822 (0.728 ~ 0.917)	0.750 (0.662 ~ 0.838)	0.833 (0.758 ~ 0.908)	0.777	0.674
	Model3	0.728 (0.614 ~ 0.842)	0.885 (0.821 ~ 0.949)	0.515 (0.414 ~ 0.616)	0.755	0.470
	Model4	0.935 (0.877 ~ 0.992)	0.901 (0.841 ~ 0.961)	0.878 (0.812 ~ 0.944)	0.894	0.664
Validation Cohort	Model1	0.821 (0.690 ~ 0.952)	0.743 (0.655 ~ 0.831)	0.867 (0.798 ~ 0.936)	0.780	0.635
	Model2	0.767 (0.609 ~ 0.925)	0.771 (0.686 ~ 0.856)	0.667 (0.572 ~ 0.762)	0.736	0.674
	Model3	0.657 (0.494 ~ 0.820)	0.600 (0.501 ~ 0.699)	0.733 (0.644 ~ 0.822)	0.660	0.470
	Model4	0.876 (0.781 ~ 0.972)	0.800 (0.719 ~ 0.881)	0.833 (0.758 ~ 0.908)	0.811	0.664

radiomics studies reported on LNM for GC. In this study, the radiomics features from perigastric fat adjacent to the tumor demonstrated significant predictive value for LNM in GC, with the model based on ID images showing superior predictive performance. That's probably because ID images can directly reflect dynamic changes in iodine concentration, effectively capturing microenvironmental changes in perigastric fat among GC patients with LNM.

However, we also found that the diagnostic performance of tumor-based radiomics model was higher than that of fat-based radiomics model, which may be due to the fact that the changes of adipose tissue may be affected by many other factors (such as nutritional status, systemic metabolism, etc.), and thus may not fully reflect the cellular heterogeneity and biological behavior of tumors. However, when the radiomics features of tumor and fat are integrated, higher predictive and application value for LNM of GC can be obtained. More and more studies have shown that molecular signaling between tumor cells and adipocytes in the tumor, around the tumor, and even distant sites plays a key role in promoting tumor growth and metastasis [25]. Therefore, the combination of radiomics features of the two can more comprehensively reflect the changes in tumor heterogeneity and invasiveness caused by the interaction of the two factors. Li Yang et al. [26] established a radiomics model combining tumoral and peritumoral radiomics features derived from DECT, showing higher diagnostic efficacy for serosal invasion in gastric adenocarcinoma than the tumor-based model alone. This conclusion is similar to that of the present study.

Numerous studies have demonstrated the extracellular stroma of tumour can comprehensively reflect the tumour microenvironment and serves as a reliable indicator for predicting invasiveness and prognosis [27]. The quantification of extracellular matrix is expressed as fECV, which has emerged as a non-invasive method for disease assessment based on imaging methods in recent years [28]. DLCT ID images directly show iodine distribution during the equilibrium phase, allowing fECV values to be calculated using single-phase images [29, 30]. Fukukura et al. [29] used equilibrium phase ID images to quantify fECV in pancreatic ductal adenocarcinoma, as an independent prognostic indicator for survival in chemotherapy patients, with higher values indicating a poorer prognosis. In our study, we obtained ECV_{ID} using the same method and observed significantly higher values in GC lesions with LNM compared to those without. Consistent with previous research, this study found that increased ECV_{ID} values in cancerous lesions indicate heightened invasiveness, likely due to excessive extracellular matrix deposition, inflammatory cell infiltration, fibroblast activation and enrichment, and vascular leakage from incomplete neovascularization within the basement membrane [31, 32]. Therefore, this study integrated ECV_{ID} into Nct and radiomics features from tumor and perigastric fat to create a nomogram, demonstrating superior predictive performance and clinical applicability.

In this study, potential sources of variability (such as the settings of spectral CT scan parameters, differences in patient characteristics, and variations in researchers' expertise) may significantly impact the results. To reduce these differences and improve the reproducibility and reliability of the research, we will first standardize the scanner settings in advance (such as resolution, contrast, and scan time) to ensure that all enrolled patients are scanned using the same settings. Second, we will use computer randomization for grouping enrolled patients to minimize differences in characteristics (such as age, gender, medical history, etc.) between the training and validation groups. Additionally, we will ensure that all researchers involved in data collection

receive the same training and follow standard operating procedures to reduce human error. Finally, we will consider potential confounding variables in data analysis and use multivariable regression statistical methods to control the impact of these variables.

There are limitations to our study: (1) The sample size is insufficient to establish a test cohort. However, we enhanced the reliability of our conclusions by employing the Bootstrap method with 1000 resampling iterations to validate each model; (2) This study was conducted at a single centre, and it is necessary to incorporate multi-centre cases for validation to enhance the robustness of our findings and expand on the clinical applicability of the findings; (3) Although previous studies have used a distance of 5 mm outside the serosa as a criterion for defining perigastric fat of GC [26], there is no established method for accurately measuring imaging features of perigastric fat, limiting its clinical applicability. Future investigations should compare different distances to define perigastric fat more precisely.

In conclusion, the nomogram integrating Nct, ECV_{ID} and radiomics models based on the tumour and perigastric fat of gastric adenocarcinoma on DLCT, demonstrated significant predictive value and offered substantial clinical utility in the preoperative assessment of LNM in GC.

Supplementary Information The online version contains supplementary material available at https://doi.org/10.1007/s00261-025-04807-0.

Author contributions Zhen Zhang, Xiaoping Zhao and Jingfeng Gu carried out the studies, participated in collecting data, and drafted the manuscript. Xuelian Chen, Hongyan Wang and Simin Zuo performed the statistical analysis and participated in its design. Mengzhe Zuo and Jianliang Wang participated in acquisition, analysis, or interpretation of data and draft the manuscript. All authors read and approved the final manuscript.

Funding KS2209/Science and Technology Project of Kunshan City. KRY-YN2022015/Guangren Foundation Research Project. SKY2022077/The program for Medical and Health Science and Technology Innovation of Suzhou. KRY-YN034/2021 Science and Technology Project of Kunshan First People's Hospital.

Data availability No datasets were generated or analysed during the current study.

Declarations

Competing interests The authors declare no competing interests.

References

1. Pan Z, Zhang H, Yan C, et al. (2010) Determining gastric cancer resectability by dynamic MDCT. Eur Radiol. 20:613–620. https://doi.org/10.1007/s00330-009-1576-2
2. Kumano S, Murakami T, Kim T, et al. (2005) T staging of gastric cancer: role of multi-detector row CT. Radiology. 237:961–966. https://doi.org/10.1148/radiol.2373041380
3. Saito H, Fukumoto Y, Osaki T, et al. (2007) Prognostic significance of level and number of lymph node metastases in patients with gastric cancer. Ann Surg Oncol. 14:1688–1693. https://doi.org/10.1245/s10434-006-9314-3
4. Shen L, Shan YS, Hu HM, et al. (2013) Management of gastric cancer in Asia: resource-stratified guidelines. Lancet Oncol. 14:e535-547. https://doi.org/10.1016/s1470-2045(13)70436-4
5. Fairweather M, Jajoo K, Sainani N, Bertagnolli MM, Wang J (2015) Accuracy of EUS and CT imaging in preoperative gastric cancer staging. J Surg Oncol. 111:1016–1020. https://doi.org/10.1002/jso.23919
6. Saito T, Kurokawa Y, Takiguchi S, et al. (2015) Accuracy of multidetector-row CT in diagnosing lymph node metastasis in patients with gastric cancer. Eur Radiol. 25:368–374. https://doi.org/10.1007/s00330-014-3373-9
7. Yang L, Shi G, Zhou T, Li Y, Li Y (2015) Quantification of the Iodine Content of Perigastric Adipose Tissue by Dual-Energy CT: A Novel Method for Preoperative Diagnosis of T4-Stage Gastric Cancer. PLoS One. 10:e0136871. https://doi.org/10.1371/journal.pone.0136871
8. Adams LC, Jurmeister P, Ralla B, et al. (2019) Assessment of the extracellular volume fraction for the grading of clear cell renal cell carcinoma: first results and histopathological findings. Eur Radiol. 29:5832–5843. https://doi.org/10.1007/s00330-019-06087-x
9. Gao L, Lu X, Wen Q, Hou Y (2021) Added value of spectral parameters for the assessment of lymph node metastasis of lung cancer with dual-layer spectral detector computed tomography. Quant Imaging Med Surg. 11:2622–2633. https://doi.org/10.21037/qims-20-1045
10. Zoico E, Rizzatti V, Darra E, et al. (2017) Morphological and Functional Changes in the Peritumoral Adipose Tissue of Colorectal Cancer Patients. Obesity (Silver Spring). 25 Suppl 2:S87-s94. https://doi.org/10.1002/oby.22008
11. Lin YC, Lin G, Yeh TS (2021) Visceral-to-subcutaneous fat ratio independently predicts the prognosis of locally advanced gastric cancer----- highlighting the role of adiponectin receptors and PPARα, β/ δ, ɤ. Eur J Surg Oncol. 47:3064–3073. https://doi.org/10.1016/j.ejso.2021.04.028
12. Park HS, Kim HS, Beom SH, et al. (2018) Marked Loss of Muscle, Visceral Fat, or Subcutaneous Fat After Gastrectomy Predicts Poor Survival in Advanced Gastric Cancer: Single-Center Study from the CLASSIC Trial. Ann Surg Oncol. 25:3222–3230. https://doi.org/10.1245/s10434-018-6624-1
13. Aerts HJ (2016) The Potential of Radiomic-Based Phenotyping in Precision Medicine: A Review. JAMA Oncol. 2:1636–1642. https://doi.org/10.1001/jamaoncol.2016.2631

14. Lambin P, Leijenaar RTH, Deist TM, et al. (2017) Radiomics: the bridge between medical imaging and personalized medicine. Nat Rev Clin Oncol. 14:749–762. https://doi.org/10.1038/nrclinonc.2017.141
15. Li J, Fang M, Wang R, et al. (2018) Diagnostic accuracy of dual-energy CT-based nomograms to predict lymph node metastasis in gastric cancer. Eur Radiol. 28:5241–5249. https://doi.org/10.1007/s00330-018-5483-2
16. Lee JW, Kim SY, Han SW, et al. (2021) Clinical Significance of Peritumoral Adipose Tissue PET/CT Imaging Features for Predicting Axillary Lymph Node Metastasis in Patients with Breast Cancer. J Pers Med. 11. https://doi.org/10.3390/jpm11101029
17. Jayaprakasam VS, Paroder V, Gibbs P, et al. (2022) MRI radiomics features of mesorectal fat can predict response to neoadjuvant chemoradiation therapy and tumor recurrence in patients with locally advanced rectal cancer. Eur Radiol. 32:971–980. https://doi.org/10.1007/s00330-021-08144-w
18. Amin MB, Greene FL, Edge SB, et al. (2017) The Eighth Edition AJCC Cancer Staging Manual: Continuing to build a bridge from a population-based to a more "personalized" approach to cancer staging. CA Cancer J Clin. 67:93–99. https://doi.org/10.3322/caac.21388
19. Jiang Y, Wang W, Chen C, et al. (2019) Radiomics Signature on Computed Tomography Imaging: Association With Lymph Node Metastasis in Patients With Gastric Cancer. Front Oncol. 9:340. https://doi.org/10.3389/fonc.2019.00340
20. Li J, Dong D, Fang M, et al. (2020) Dual-energy CT-based deep learning radiomics can improve lymph node metastasis risk prediction for gastric cancer. Eur Radiol. 30:2324–2333. https://doi.org/10.1007/s00330-019-06621-x
21. Rybinska I, Mangano N, Tagliabue E, Triulzi T (2021) Cancer-Associated Adipocytes in Breast Cancer: Causes and Consequences. Int J Mol Sci. 22. https://doi.org/10.3390/ijms22073775
22. Duong MN, Geneste A, Fallone F, Li X, Dumontet C, Muller C (2017) The fat and the bad: Mature adipocytes, key actors in tumor progression and resistance. Oncotarget. 8:57622–57641. https://doi.org/10.18632/oncotarget.18038
23. Kalezic A, Udicki M, Srdic Galic B, et al. (2021) Tissue-Specific Warburg Effect in Breast Cancer and Cancer-Associated Adipose Tissue-Relationship between AMPK and Glycolysis. Cancers (Basel). 13. https://doi.org/10.3390/cancers13112731
24. Xiao J, Shen K, Liu K, et al. (2022) Obesity promotes lipid accumulation in lymph node metastasis of gastric cancer: a retrospective case–control study. Lipids Health Dis. 21:123. https://doi.org/10.1186/s12944-022-01734-7
25. Neto NIP, Murari ASP, Oyama LM, et al. (2018) Peritumoural adipose tissue pro-inflammatory cytokines are associated with tumoural growth factors in cancer cachexia patients. J Cachexia Sarcopenia Muscle. 9:1101–1108. https://doi.org/10.1002/jcsm.12345
26. Yang L, Sun J, Yu X, et al. (2022) Diagnosis of Serosal Invasion in Gastric Adenocarcinoma by Dual-Energy CT Radiomics: Focusing on Localized Gastric Wall and peritumoral Radiomics Features. Front Oncol. 12:848425. https://doi.org/10.3389/fonc.2022.848425
27. Sangaletti S, Chiodoni C, Tripodo C, Colombo MP (2017) Common extracellular matrix regulation of myeloid cell activity in the bone marrow and tumor microenvironments. Cancer Immunol Immunother. 66:1059–1067. https://doi.org/10.1007/s00262-017-2014-y
28. Shao R. (2020) Extracellular volume fraction based on contrast-enhanced CT images predicts hepatic metastasis and lymphatic metastasis from colon carcioma. Jilin University.
29. Fukukura Y, Kumagae Y, Higashi R, et al. (2020) Extracellular volume fraction determined by equilibrium contrast-enhanced dual-energy CT as a prognostic factor in patients with stage IV pancreatic ductal adenocarcinoma. Eur Radiol. 30:1679–89. https://doi.org/10.1007/s00330-019-06517-w
30. Aslan S, Camlidag I, Nural MS. (2019) Lower energy levels and iodine-based material decomposition images increase pancreatic ductal adenocarcinoma conspicuity on rapid kV-switching dual-energy CT. Abdom Radiol (NY). 44:568–75. https://doi.org/10.1007/s00261-018-1754-2
31. Erdogan B, Webb DJ (2017) Cancer-associated fibroblasts modulate growth factor signaling and extracellular matrix remodeling to regulate tumor metastasis. Biochem Soc Trans. 45:229–236. https://doi.org/10.1042/bst20160387
32. Mathivet T, Bouleti C, Van Woensel M, et al. (2017) Dynamic stroma reorganization drives blood vessel dysmorphia during glioma growth. EMBO Mol Med. 9:1629–1645. https://doi.org/10.15252/emmm.201607445